FE ANALYSIS OF DAMAGE EVOLUTION DURING THE DEEP DRAWING OF TEXTURED ALUMINUM SHEETS

JianGuo HU[a], Takashi ISHIKAWA[a], John. J. JONAS[b], Nobuki YUKAWA[a] and Keisuke IKEDA[c]

[a]*Department of Materials Processing, School of Engineering, Nagoya University, 464-8603 Japan*
[b]*Department of Metallurgical Engineering, McGill University, Montreal, H3A 2B2 Canada*
[c]*Department of Materials Processing, School of Engineering, Tohoku University, 980-8579 Japan*

ABSTRACT Void nucleation and growth models have been incorporated into an elasto-plastic finite element code together with an anisotropic fourth-order strain-rate potential so that damage evolution during the deep drawing of textured aluminum sheets can be analyzed. The fourth-order strain-rate potential is based on the Taylor model of crystal plasticity and therefore takes the presence of texture into account. Damage evolution is modelled in terms of void nucleation and growth during deformation. Strain-induced and stress-controlled nucleation models were employed in conjuction with the Cocks and Ashby growth model to calculate the increase in void volume fraction. The influence of plastic anisotropy on damage is discussed together with the roles of void nucleation and growth on damage evolution for cold-rolled and annealed aluminum sheets.

Keywords: *damage, texture, void nucleation and growth, finite element simulation, sheet forming*

1. INTRODUCTION

A variety of microstructural changes occur during plastic deformation. Some of these can lead to the degradations in mechanical properties commonly known as *damage*. Coffin and Rogers [1] have described such damage in terms of microvoid formation at inclusions, grain boundaries and regions of high deformation gradient. Such microvoids are generally nucleated at rather small strains and grow by ductile deformation, eventually coalescing with other microvoids to form an elongated void of observable size (larger than 1 μm). The propagation of such elongated voids results in ductile fracture. Internal deterioration by void nucleation and growth around inclusions has therefore been termed ductile fracture damage. More recently, Hu *et al.* [2] demonstrated that there is a significant effect of damage evolution (void nucleation and growth) on the limit strain in biaxially stretched aluminum alloy sheets.

In this work, an elasto-plastic finite element (ABAQUS) code is employed, together with an texture-based anisotropic fourth-order strain-rate potential, void nucleation and growth models to simulate the damage evolution that takes place in textured aluminum sheets during deep drawing. The fourth-order strain-rate potential is based on the Taylor model of crystal plasticity and therefore takes texture into account. Damage evolution is modeled in terms of void nucleation and growth during

deformation. A strain-induced and stress-controlled nucleation models are used in conjunction with the Cocks and Ashby growth model to analyze the increase in void volume fraction. The influence of plastic anisotropy on damage is discussed together with that of void nucleation and growth on damage evolution for rolled and annealed aluminum sheets.

2. ANALYTICAL METHOD

2.1 Damage variables

The increase in void volume fraction can be written as

$$\dot{f} = \dot{f}_n + \dot{f}_g \qquad (1)$$

where $\dot{f}_n$ and $\dot{f}_g$ denote the increases associated with the nucleation of new voids and with the growth of existing voids.

The second phase particles present in conventional metals and alloys are the primary sources of internal voids, at least at temperatures near room temperature, although other void nucleation sites may contribute in certain circumstances. Voids are initiated either by cracking of the particles or by decohesion of the particle-matrix interface. When voids are assumed to grow as spherical cavities after nucleation, the void fraction increment during deformation can be given as follows:

$$\dot{f}_n = M_1 \dot{\bar{\sigma}} + M_2 (\dot{\sigma}_m) \qquad (2)$$

Here, the parameters M_1 and M_2 represent the dependences of the nucleation rate on the increment in the flow stress ($\bar{\sigma}$) in the matrix and on the increment of hydrostatic stress (σ_m), respectively.

2.2 Strain induced void nucleation

Based on Gurson's assumption of plastic strain controlled void nucleation [3], Goods and Brown [4] reviewed the micromechanics of void nucleation and then neglected the effect of hydrostatic stress so that they could reduce the above equation (2) to

$$\dot{f}_n = M_1 \dot{\bar{\sigma}} = F \dot{\varepsilon}_e^p \qquad (3)$$

Where $\dot{\varepsilon}_e^p$ is the equivalent plastic strain rate and F depends on the plastic strain history as well as on the statistics of the second phase particle distribution. With respect to the latter, Chu and Needleman [5] suggested and adopted the simple idealization that there is a mean equivalent plastic strain for void nucleation, ε_n. Thus, the so-called strain induced void nucleation model can be expressed as follows:

$$F = \frac{\varphi}{s\sqrt{2\pi}} \exp\left(-\frac{1}{2} \left(\frac{\varepsilon_e^p - \varepsilon_n}{s} \right)^2 \right) \qquad (4)$$

where s is the standard deviation of the distribution and φ is selected so that the total void volume nucleated is consistent with the volume fraction of second phase particles. By varying the standard deviation, s, models with a variable range of strains over which most of the voids nucleate can be obtained. Some recent studies (e.g. [6] in an Al-Mn alloy) have found that void nucleation can occur next to certain small particles within a very narrow range of strain.

2.3 Stress controlled void nucleation

Argon *et al.* [7] suggested that the nucleation criterion depends only on the maximum stress transmitted across the particle-matrix interface. They assumed that the maximum stress can be approximated by $(\bar{\sigma}+\sigma_m)$. Based on an extension of their consideration of the statistics of the second phase particle distribution, Gurson [8] proposed an elaborate nucleation model, which was called the stress controlled void nucleation model. It is expressed as follows:

$$\dot{f}_n = K(\dot{\bar{\sigma}} + \sigma_m) \qquad (5)$$

where K relies on the deformation and hydrostatic stress history and can be given by the expression:

$$K = \frac{\varphi}{s\sigma_y\sqrt{2\pi}}\exp\left(-\frac{1}{2}\left(\frac{\bar{\sigma}+\sigma_m-\sigma_n}{s\sigma_y}\right)^2\right) \qquad (6)$$

Here σ_y is the matrix yield strength and σ_n is the mean value in a normal distribution.

2.4 Cocks and Ashby's void growth model

The growth of voids was modeled by the damage model proposed by Cocks and Ashby [8, 9] and the conservation of mass equation was modified to accommodate the volumetric deformation due to the accumulation of damage. This damage model identifies the dominant growth mechanism of voids as transgranular creep of the surrounding material matrix. The model assumes that, under creep conditions, damage in the metal occurs by the growth and coalescence of the voids that lie within grains and on the grain boundaries. The simplified evolution equation for the accumulation of damage is given by

$$\dot{f}_g = \beta(n,\sigma_m,\sigma'_{II})\left[\frac{1}{(1-f_g)^n}-(1-f_g)\right]\dot{\varepsilon}^p_e \qquad (7)$$

where the stress function

$$\beta = \sinh\left(2\frac{2n-1}{2n+1}\frac{\sigma_m}{\sigma'_{II}}\right) \qquad (8)$$

The parameter β accounts for the influence of stress state and σ'_{II} is the Mises equivalent stress. As the term σ_m/σ'_{II} increases, the hydrostatic component of the stress tensor dominates more and more and voids grow more quickly. The parameter β is also intended to accommodate the effect of the shape change of the voids on the evolution of the internal porosity. In this growth model, only one model parameter, n is required to compute the evolution of the internal porosity. Cocks and Ashby have indicated that the calculated results are well fitted by the void growth formula whenever $3 \le n \le 8$. In this analysis, we have taken n to be 5.0 for calculations. The damage model of Cocks and Ashby does not take into account the *nucleation* of voids. Damage accumulates only due to the growth of existing voids. Therefore, a small amount of damage (internal porosity) must exist initially for the damage to grow.

2.5 Fourth-order strain-rate potential

The fourth-order strain rate potential used in the present work has the following form [11, 12]:

$$\psi(\dot{E}^P) = \sum_{K=1}^{22} \alpha_K \frac{X_K(\dot{E}^P)}{||\dot{E}^P||^3} \qquad (9)$$

where $$[\dot{E}^p]^T = [\dot{\varepsilon}^p_{11}, \dot{\varepsilon}^p_{22}, \dot{\varepsilon}^p_{12}, \dot{\varepsilon}^p_{13}, \dot{\varepsilon}^p_{23}] \qquad (10)$$

$X_1 = (\dot{\varepsilon}^p_{11})^4$ $X_2 = (\dot{\varepsilon}^p_{22})^4$ $X_3 = (\dot{\varepsilon}^p_{23})^4$ $X_4 = (\dot{\varepsilon}^p_{13})^4$

$X_5 = (\dot{\varepsilon}^p_{12})^4$ $X_6 = (\dot{\varepsilon}^p_{11})^3 \dot{\varepsilon}^p_{22}$ $X_7 = (\dot{\varepsilon}^p_{22})^3 \dot{\varepsilon}^p_{11}$ $X_8 = (\dot{\varepsilon}^p_{11})^2 (\dot{\varepsilon}^p_{22})^2$

$X_9 = (\dot{\varepsilon}^p_{11})^2 (\dot{\varepsilon}^p_{23})^2$ $X_{10} = (\dot{\varepsilon}^p_{11})^2 (\dot{\varepsilon}^p_{13})^2$ $X_{11} = (\dot{\varepsilon}^p_{11})^2 (\dot{\varepsilon}^p_{12})^2$ $X_{12} = (\dot{\varepsilon}^p_{22})^2 (\dot{\varepsilon}^p_{23})^2$

$X_{13} = (\dot{\varepsilon}^p_{22})^2 (\dot{\varepsilon}^p_{13})^2$ $X_{14} = (\dot{\varepsilon}^p_{22})^2 (\dot{\varepsilon}^p_{12})^2$ $X_{15} = (\dot{\varepsilon}^p_{23})^2 (\dot{\varepsilon}^p_{13})^2$ $X_{16} = (\dot{\varepsilon}^p_{23})^2 (\dot{\varepsilon}^p_{12})^2$

$X_{17} = (\dot{\varepsilon}^p_{13})^2 (\dot{\varepsilon}^p_{12})^2$ $X_{18} = \dot{\varepsilon}^p_{11}\dot{\varepsilon}^p_{22}(\dot{\varepsilon}^p_{23})^2$ $X_{19} = \dot{\varepsilon}^p_{11}\dot{\varepsilon}^p_{22}(\dot{\varepsilon}^p_{13})^2$ $X_{20} = \dot{\varepsilon}^p_{11}\dot{\varepsilon}^p_{22}(\dot{\varepsilon}^p_{12})^2$

$X_{21} = \dot{\varepsilon}^p_{11}\dot{\varepsilon}^p_{23}\dot{\varepsilon}^p_{13}\dot{\varepsilon}^p_{12}$ $X_{22} = \dot{\varepsilon}^p_{22}\dot{\varepsilon}^p_{23}\dot{\varepsilon}^p_{13}\dot{\varepsilon}^p_{12}$

and $$||\dot{E}^p|| = \sqrt{2}\{(\dot{\varepsilon}^p_{11})^2 + (\dot{\varepsilon}^p_{22})^2 + \dot{\varepsilon}^p_{11}\dot{\varepsilon}^p_{22} + (\dot{\varepsilon}^p_{12})^2 + (\dot{\varepsilon}^p_{13})^2 + (\dot{\varepsilon}^p_{23})^2\}^{1/2} \qquad (11)$$

Five independent components of the plastic strain rate tensor ($\dot{\varepsilon}^p_{11}$, $\dot{\varepsilon}^p_{22}$, $\dot{\varepsilon}^p_{12}$, $\dot{\varepsilon}^p_{23}$, ε^p_{13}), exist on the basis of the incompressibility of plastic deformation. The strain rate potential is a homogeneous function of degree one with respect to positive multipliers. Orthotropic symmetry is assumed, so that the potential is only suitable for textures with this type of symmetry. However, the effect of voids on the potential function was neglected in this work.

3. SIMULATIONS

In order to examine the effect of texture on damage, two kinds of aluminum sheets, cold-rolled and, cold-rolled and annealed, were selected for deep drawing simulations. Both were cold-rolled to a reduction of 90%, and the annealed sheets were treated at 623K for one hour after cold-rolling. A more detailed description of their treatment and the measurement of their mechanical properties and pole figures was reported elsewhere [13]. The ODFs of the two kinds of aluminum sheets are shown in **Fig. 1**.

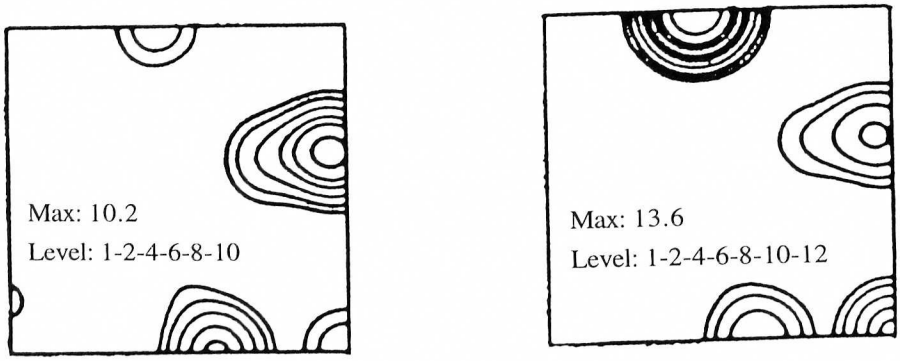

(a) Cold-rolled 90% **(b)** Cold-rolled 90% and annealed

Figure 1 ODFs for the present aluminum sheets ($\varphi_2 = 45^0$ sections).

As presented in **Fig. 1 (a)**, there is a relatively strong rolling texture in the cold-rolled sheet, which consists mainly of the *brass*, *S* and *copper* components. In **Fig. 1 (b)**, there is a mixture of a quite

strong *cube* component and some weak retained-rolling components (*brass*, *S* and *copper*) in the annealed sheet; this mixture is typical of recrystallization textures in aluminum sheets.

Blanks 78mm in diameter and 1.0mm in thickness were employed in the simulations. Eight-node linear brick elements with reduced integration and hourglass control (known as C3D8R in ABAQUS terminology) were adopted with one layer through the thickness of a blank. Because of the orthotropic sample symmetry, only a quarter of the blank was used for modelling. The numbers of elements and nodes are 112 and 266, respectively. The full geometry of cup drawing and friction between the tools and the blank were taken into consideration in these simulations. The geometry of the tools was described elsewhere [14].

4. RESULTS and DISCUSSION

In order to analyze damage evolution during deep drawing, the separate influences of strain induced nucleation, stress controlled nucleation, and of the growth of initial voids on the damage that develops during the various stages of a process were predicted. The results at a punch stroke level of 60% are presented in **Figs. 2** and **3** for the cold-rolled and cold-rolled and annealed aluminum sheets, respectively.

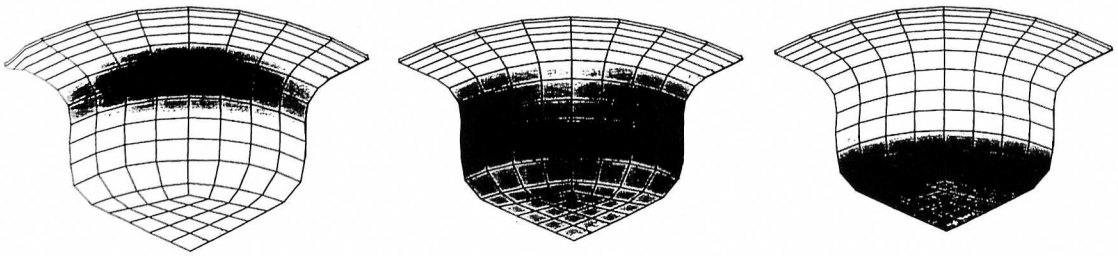

(a) Strain induced nucleation (b) Stress controlled nucleation (c) Cocks & Ashby void growth

Figure 2 Damage evolution obtained from the various models for the cold-rolled aluminum sheet.

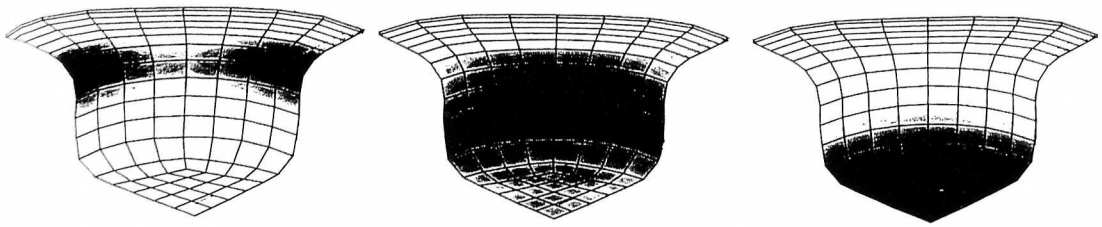

(a) Strain induced nucleation (b) Stress controlled nucleation (c) Cocks & Ashby void growth

Figure 3 Damage evolution obtained from the various models for the annealed aluminum sheet.

4.1 Damage calculated from the strain induced nucleation model

As shown in **Figs. 2 (a)** and **3 (a)**, the maximum in damage for the cold-rolled sheet occurs at 45^0 from the RD (rolling direction) near the die radius area; whereas the maxima for the annealed sheet are at 0 and 90^0 near the die radius area. It is evident that the location of the maximum damage

zone obtained from the strain induced nucleation depends strongly on the texture and therefore on the plastic anisotropy of the sheet.

4.2 Damage calculated from the stress controlled nucleation model

Figs. 2 (b) and **3 (b)** demonstrate that the maxima in damage predicted from the stress controlled nucleation for the two aluminum sheets are located in the middle of the wall. However, the contours are quite different for the cold-rolled as opposed to the col-rolled and annealed sheets.

4.3 Damage obtained from the growth of initial voids

The damage contour obtained from the growth model for initial voids are displayed in **Figs. 2 (c)** and **3 (c)** for the cold-rolled and cold-rolled and annealed sheets, respectively. Their maxima are located in the punch radius area, and the two sheets exhibit similar patterns. It can be seen that plastic anisotropy has an insignificant influence on the growth of initial voids.

5. CONCLUSIONS

Based on an elasto-plastic finite element (ABAQUS) code, and a texture-based anisotropic fourth-order strain-rate potential, void nucleation and growth models have been employed to model the damage evolution that takes place in textured aluminum sheets during deep drawing. The agreement between predictions and observations demonstrates that such simulations are effective for the analysis of damage evolution and for the prediction of the occurrence of fracture during deep drawing.

Acknowledgments

The authors are grateful to Dr. Y. Zhou (Suralform Aluminum International Limited, Canada) as well as to Drs. J. Savoie and S. MacEwen (KRDC, Alcan International Limited, Canada) for their helpful discussions and encouragement.

REFERENCES:

[1] L. F. Coffin Jr. and H. C. Rogers: *Transactions of the ASME*, **62** (1967), 672.

[2] J. Hu, J. J. Jonas and T. Ishikawa: Proc. of Fourth AEPA, Seoul, June 21-25 (1998), in press.

[3] A. L. Gurson: *J. Eng. Mater. Tech, ASME*, **99** (1977), 2.

[4] S. H. Goods and L. M. Brown: *Acta Metallurgica*, **27** (1979), 1.

[5] C. C. Chu and A. Needleman: *J. Engineering Materials and Technology*, **102** (1980), 249.

[6] A. Melander: *Scandinavian Journal of Metallurgy*, **8** (1979), 99.

[7] A. S. Argon, J. Im and R. Sofoglu: *Metallurgical Transactions*, **6A** (1975), 825.

[8] A. L. Gurson: **Fracture** (eds. D. M. R. Taplin), Univ. Waterloo Press, **2** (1977), p357.

[9] A. C. F. Cocks and M. F. Ashby: *Met. Sci.*, **14** (1980), 395.

[10] A. C. F. Cocks and M. F. Ashby: **Creep in Structures** (eds. A. R. S. Ponter and D. R. Hayhurst), Springer, Berlin, (1980), p368.

[11] M. Arminjon and B. Bacroix: *Acta Mechanica*, **88** (1991), 219.

[12] Y. Zhou, J. J. Jonas, L. Szabo, A. Makinde, M. Jain and S. MacEwen: *Int. J. Plasticity*, **9** (1997), 165.

[13] J. Hu, K. Ikeda and T. Murakami: *J. Japan Institute of Metals*, **60** (1996), 1130.

[14] J. Hu, T. Ishikawa, J. J. Jonas and K. Ikeda: *Mater. Trans, JIM*, **39** (1998), 469.